

Influence of bias voltage noise on the Inelastic Cooper-Pair Tunneling Amplifier (ICTA)

U. Martel,¹ R. Albert,² F. Blanchet,² J. Griesmar,¹ G. Ouellet,¹ H. Therrien,¹ N. Nehra,¹ N. Bourlet,¹ and M. Hofheinz¹

¹*Institut Quantique, Université de Sherbrooke, Sherbrooke, Québec, Canada J1K 2R1*

²*Univ. Grenoble Alpes, CEA, INAC-PHELIQS, F-38000 Grenoble, France*

(*Electronic mail: max.hofheinz@usherbrooke.ca)

(Dated: 30 September 2024)

We experimentally show that the Inelastic Cooper-Pair Tunneling Amplifier (ICTA), implementing a DC-powered parametric amplification scheme, can achieve gain and noise performance similar to that of Josephson parametric amplifiers. Using experimental data and simulations, we show that the ICTA has near-quantum-limited noise as long as the integral voltage bias noise divided by the superconducting flux quantum is below the amplification bandwidth. We observe a gain of 20 dB with noise below 1.7 times the quantum limit when the full width at half maximum of the integral voltage noise, expressed as frequency, is 5.6 MHz.

Superconducting parametric amplifiers have been one of the major driving forces behind the success of circuit QED and quantum computing with superconducting circuits and have also enabled progress in many other fields¹. They allow quantum limited amplification and exist in a wide variety of configurations such as resonant amplifiers²⁻⁵ or traveling wave amplifiers (TWPAs)⁶⁻¹¹.

However, these parametric amplifiers are powered by a strong AC pump tone which requires hardware overhead for generation and routing. In addition, the pump tone may perturb the device under test or saturate the subsequent readout chain. Filtering this tone usually requires additional hardware overhead in the form of circulators, diplexers and filters which cause loss in the signal path, degrading the system noise performance. DC-powered superconducting amplifiers using Josephson junctions such as the SLUG¹² and the SJA¹³ do away with the AC pump, but they suffer from higher noise because they lack a well-defined cool idler mode.

We have previously demonstrated that it is possible to implement a parametric amplification scheme in Josephson photonics based on inelastic Cooper pair tunneling¹⁴. This DC powered Inelastic-Cooper-pair-Tunneling Amplifier (ICTA) allows for a well-identified cold idler mode which, theoretically, allows reaching the quantum limit. Nonetheless, the first implementation of this device¹⁴ wasn't able to reach gains higher than approximately 10 dB while keeping noise within a factor 2 of the quantum limit.

Here we show that the limiting factor for higher gains is low-frequency noise on the voltage bias, which is equivalent to phase noise of the pump tone in JPAs. The general idea is that the window of optimal bias voltage is closely related to the bandwidth of the amplifier and becomes narrower with increasing gain. When it becomes narrower than the low-frequency voltage noise, instantaneous gain below the optimal gain becomes increasingly likely. The average power gain is then $\langle S_{aa} \rangle^2$, where S_{aa} is the instantaneous amplitude gain. If the amplifier is quantum limited at each instant, the average output noise is $\langle |S_{aa}|^2 - 1 \rangle$. As $\langle S_{aa} \rangle^2 < \langle |S_{aa}|^2 \rangle$ unless S_{aa} is constant, the voltage fluctuations reduce gain more strongly than noise, degrading the input-referred noise. Therefore, voltage noise limits the maximal gain that can be achieved while maintaining noise close to the quantum limit.

We first derive the relation of gain, bandwidth and optimal bias-voltage range of the ICTA and then show that they explain the experimental amplifier noise for different gains and bias-voltage noises.

The ICTA circuits we consider are shown in Fig. 1a and b and consist of a Josephson junction biased at a Josephson frequency ω_J with Josephson energy E_J and phase ϕ , in series with two

resonators of frequencies ω_a and ω_b . The corresponding ICTA Hamiltonian is^{15,16}

$$H = \hbar\omega_a a^\dagger a + \hbar\omega_b b^\dagger b - E_J \cos(\phi) \quad (1)$$

with

$$\phi = \omega_J t + \varphi_a(a^\dagger + a) + \varphi_b(b^\dagger + b)$$

where $\omega_J = 2eV/\hbar$ is the Josephson frequency, and $\varphi_{a,b} = \sqrt{\pi \frac{4e^2}{\hbar} Z_{a,b}}$ are the zero-point fluctuations of phase of modes $\omega_{a,b}$, with $Z_{a,b}$ their characteristic impedances.

Supposing small signals and low $\varphi_{a,b}$ we can develop the cosine term,

$$-E_J \cos(\phi) = -\frac{E_J}{2} [e^{i\omega_J t} e^{i\varphi_a(a^\dagger + a)} e^{i\varphi_b(b^\dagger + b)} + \text{h.c.}], \quad (2)$$

to second order in $\varphi_a a$ and $\varphi_b b$.

Assuming low Josephson energy, i.e. $\varphi_{a,b} E_J/\hbar$ is small compared to the mode frequencies, we can perform a rotating wave approximation at $\omega_J \approx \omega_a + \omega_b$. Together, these approximations yield the well-known parametric amplifier Hamiltonian

$$H = \hbar\omega_a a^\dagger a + \hbar\omega_b b^\dagger b + \hbar\lambda (a^\dagger b^\dagger e^{-i\omega_J t} + \text{h.c.}), \quad (3)$$

with $\lambda = \frac{E_J \varphi_a \varphi_b}{2\hbar}$. It maps to the JPA Hamiltonian¹⁷ with the voltage bias ω_J and the Josephson energy E_J in the ICTA playing, respectively, the role of pump frequency and pump amplitude in the JPA.

Using input-output theory to eliminate the cavity modes in the same way as for the JPA¹⁷⁻¹⁹, we can show that

$$S_{aa} = \frac{\eta_a \eta_b + \Xi^2}{\eta_a^* \eta_b - \Xi^2} \quad (4)$$

where we have defined $\Xi = \frac{2\lambda}{\sqrt{\Gamma_a \Gamma_b}}$ with Γ_a and Γ_b being the relaxation rates of the resonators, and

$$\eta_x = 1 + 2i \frac{\Delta_x}{\Gamma_x} \quad (5)$$

with $\Delta_a = \omega_s - \omega_a$ the detuning between the signal frequency and the signal mode and $\Delta_b = \omega_J - \omega_s - \omega_b$ the detuning between the idler frequency $\omega_J - \omega_s$ and the idler mode ω_b . The maximum of gain S_{aa} reached for $\Delta_a = \Delta_b = 0$ is then

$$S_{aa}^{\max} = \frac{1 + \Xi^2}{1 - \Xi^2}. \quad (6)$$

Under optimal bias condition $\omega_J = \omega_a + \omega_b$, we have $\Delta_a = -\Delta_b = \Delta$ and in the limit of high gain, the gain profile is approximately Lorentzian

$$S_{aa} \xrightarrow{\Xi \rightarrow 1^-} \frac{S_{aa}^{\max}}{1 - iS_{aa}^{\max} \frac{\Delta}{\Gamma}}, \quad (7)$$

where $\Gamma^{-1} = \Gamma_a^{-1} + \Gamma_b^{-1}$. It follows that the bandwidth is

$$B_0 = \frac{2\Gamma}{S_{aa}^{\max}}. \quad (8)$$

If instead the input signal is kept on resonance, but the voltage bias varies, we have $\Delta_a = 0$ and $\Delta = \Delta_b = \omega_J - \omega_a - \omega_b$ and $\Gamma = \Gamma_b$ in Eqs. (7) and (8).

This means that the amplifier bandwidth and optimal bias-voltage range are of the same order of magnitude and for the degenerate case, where signal and idler reside in the same mode, the optimal bias-voltage range is exactly twice the bandwidth. Both widths are inversely proportional to the maximal gain.

The experimental setup is shown in Fig. 1c. A DC bias is applied to the ICTA through a voltage divider and filter (see Appendix A) with output impedance of either $50\ \Omega$ or $5\ \Omega$. The voltage-bias noise is dominated by the thermal noise of the cold resistor of the voltage divider and the dissipation in the low-pass filter. The different output impedances of the filters, therefore, result in different voltage-bias noise. A SQUID acts as a flux tunable Josephson junction which we use to adjust the gain of the ICTA via an on-chip flux line, biased by a room temperature voltage source in series with a $5\ \text{k}\Omega$ resistor and filtered at base temperature using a custom dissipative low-pass filter²⁰ with a cutoff frequency of the order of 200 MHz.

To measure gain, a microwave signal is sent to the sample through an attenuated line, a circulator, a switch and a high-pass filter. The circulator then routes the signal reflected from the device to a cryogenic HEMT amplifier at 4K. The signal is then further amplified, downconverted and digitized using a custom double-heterodyne receiver, phase locked to the input signal. This setup allows for scalar network analyzer measurements and noise measurements using the same signal pathway.

The switch allows us to also connect the readout chain to a short circuit and two loads, one thermally anchored to the mixing chamber stage of the fridge and one to the still stage at approximately 1 K. The microwave loads at different temperatures are used for Y-factor calibration of the noise measurement, and the short is used to calibrate the gain measurement, as detailed in Appendix B.

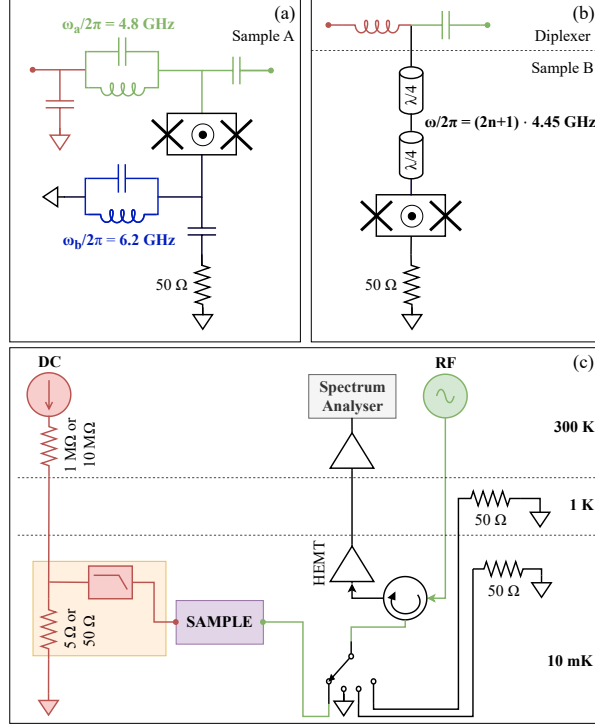


FIG. 1. Setup and sample schematics. Green is used for RF signals and red for DC. (a) Sample A, with on-chip bias-tee. (b) Sample B, with off-chip diplexer. (c) Measurement chain. The orange box is the biasing circuit (see Fig. 5 for details). The $1\text{ M}\Omega$ resistor is used with the $5\ \Omega$ biasing circuit and the $10\text{ M}\Omega$ resistor is used with the $50\ \Omega$ biasing circuit.

Fig. 1a and Fig. 1b show the two samples measured in this article. On sample A, LC resonators form the signal and idler modes. DC bias and the microwave signal are applied through separate ports, allowing further noise filtering directly on chip (see Appendix A). Signal and idler modes of Sample B are formed by a $\lambda/4$ resonator. DC and microwave signals are connected to the same port and split using an off-chip diplexer (Marki DPXN-M50) with a 50 MHz cross-over frequency. Samples are fabricated using a self-aligned process²¹ with Nb/Al/AlO_x/Nb junctions, two Nb routing layers, separated by SiN dielectric.

We thus have three different experimental configurations for voltage noise: low noise with sample A with on-chip filtering combined with the $5\ \Omega$ bias circuit, medium noise with sample B without on-chip filtering, combined with the $5\ \Omega$ bias circuit, and high noise with Sample B combined with the $50\ \Omega$ bias circuit. We characterize the voltage noise using the AC-Josephson effect. We first maximally frustrate the SQUIDs so that spontaneous emission by the devices is minimal and can be described by $P(E)$ theory^{22,23}. We then measure the power spectral density emitted

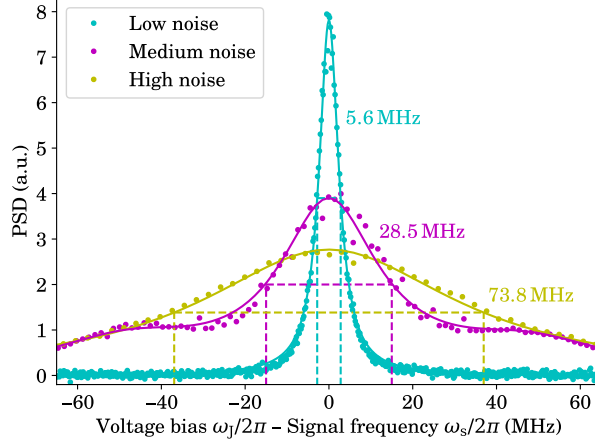


FIG. 2. Voltage noise measurement (dots) for the three configurations, through measurement of the AC Josephson effect at minimum Josephson energy E_J . Frequency $\omega_s/2\pi$ was fixed at 4772 MHz for sample A (low noise) and 4122 MHz for Sample B (medium and high noise). The low and high noise curves were each fitted (solid lines) using a single Lorentzian distribution, whereas three were needed for the medium noise curve. Dashed lines indicate FWHM of each curve. For the medium noise, the FWHM of the central peak is shown.

by the devices at a fixed frequency ω and vary the Josephson frequency ω_J around ω , giving the voltage noise distribution. If the low-frequency impedance of the Josephson junction bias Z is $\ll \frac{h}{4e^2}$ and flat up to frequencies $> kT/h$, and if the Josephson energy is low, this distribution is expected to be a Lorentzian^{23,24} with a FWHM of

$$\Delta V = \frac{h}{2e} \frac{\Delta\omega_J}{2\pi} = 4\pi k_B T \frac{2e}{h} Z(0). \quad (9)$$

Fig. 2 shows that for the low-noise configuration and high-noise configuration, the voltage noise distribution is well fitted by the expected Lorentzian shape, with full widths at half maximum of, respectively, $\Delta\omega_J/2\pi = 5.6\text{MHz}$ and $\Delta\omega_J/2\pi = 73.8\text{MHz}$, corresponding to effective temperatures of the bias resistors of, respectively, 27.6 mK and 36.4 mK. In the medium-noise configuration, additional bumps appear at $\pm 48\text{MHz}$ because the $5\ \Omega$ bias circuit is not impedance matched to the diplexer and transmission line, so that a resonance forms at the cross-over frequency of the diplexer. A combination of three Lorentzian distributions were used to fit this configuration, resulting in full widths at half maximum (FWHM) of $\Delta\omega_J/2\pi = 28.5\text{MHz}$ for the central peak and $\Delta\omega_J/2\pi = 45.8\text{MHz}$ for the two side peaks at $\pm 48\text{MHz}$.

Fig. 3 shows typical gain and noise curves for the low-noise configuration at fixed voltage bias

and for different Josephson energies tuned via the flux bias to the SQUID. Magnetic flux close to half a flux quantum, corresponding to the lowest the Josephson energy E_J , gives the lowest gain and highest bandwidths, as expected from Eq. (8). For the three lowest gain curves, the noise is virtually the same, between 1 and 1.3 times the quantum limit. Increasing the gain, and thereby reducing the bandwidth, slightly increases the noise but it remains below 1.5 and 1.7 times the quantum limit up to 18 dB and 20.5 dB, respectively.

In Fig. 4 we plot the gain, bandwidth and noise extracted from similar curves for the low noise, medium noise and high noise configurations. Data was taken by varying the Josephson energy while using a fixed voltage bias for each configuration. Like in Fig. 3, we can see in Fig. 4a that raising the gain also raises the noise. For the same gain, we see lower amplification noise with lower voltage noise. The maximum gain we can achieve while remaining below three times the quantum limit is 11.1 dB for the highest noise configuration, 14.1 dB for the medium one, and 25.6 dB for the lowest one.

We compare these experimental results with Eq. (4) averaged over the fitted voltage bias distri-

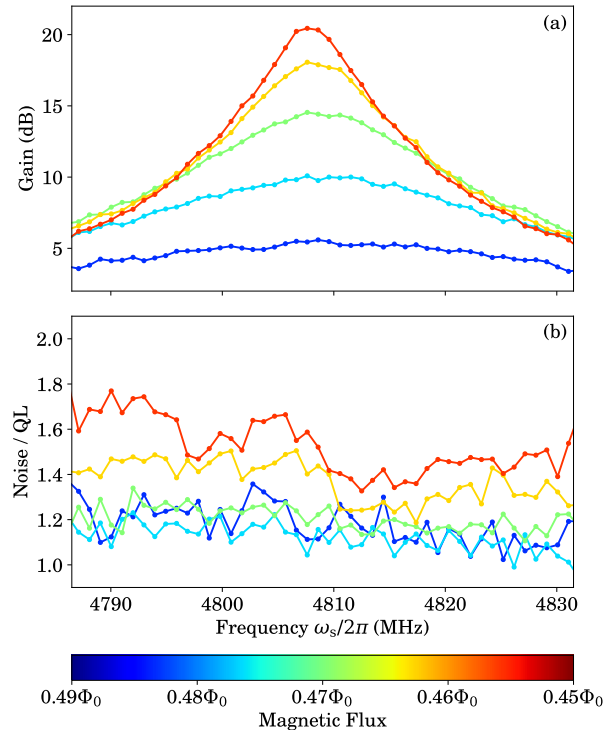


FIG. 3. Gain (a) and noise referred to the quantum limit (b) of the low noise configuration (sample A with $5\ \Omega$ bias circuit) as a function of magnetic flux and frequency for a voltage bias of $\omega_j/2\pi = 10991$ MHz, with a idler mode $\omega_b/2\pi = 6181$ MHz. (See Appendix B for details on calibration.)

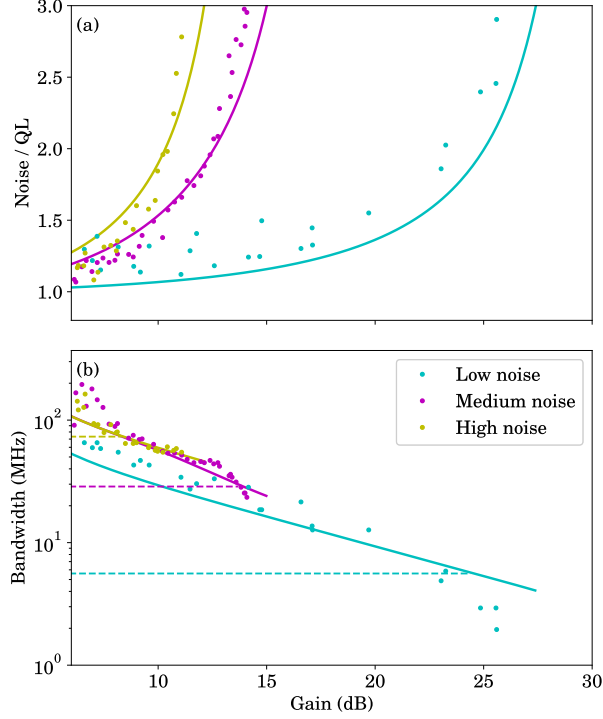


FIG. 4. Noise with respect to the quantum limit (a) and bandwidth (b) as a function of gain, adjusted via effective Josephson energy E_J , and at fixed voltage bias $\omega_J/2\pi$ at 10952 MHz for Sample A (low noise) and 8982 MHz for Sample B (medium and high noise). Signal frequency $\omega_s/2\pi$ is 4771 MHz for Sample A and 4540 MHz for Sample B. The width of the signal mode is 102 MHz and the width of the idler mode is 86 MHz for Sample A, whereas widths for the signal and idler modes are both 142 MHz for Sample B (near-degenerate amplification). Dots are measurements, solid lines correspond to an ideal parametric amplifier following Eq. (4) with quantum limited noise, averaged over the fitted voltage bias distributions (see Fig. 2), with measured signal and idler mode widths and Ξ as sweep parameter. Dashed lines are the FWHM of the corresponding voltage noise distributions.

butions determined from the data in Fig. 2, approximating the voltage bias fluctuations as adiabatic and using Ξ as a variable. These numerical calculations closely follow the experimental data without any fitting parameter, even though they slightly underestimate the noise. The slightly higher noise in the experimental results may be due to losses in the device.

Fig. 4b shows the relationship between the bandwidth and the gain. Both experimental and numerical results show the expected constant gain \times bandwidth product expected from Eq. (7). By design, Sample B has resonators with lower Q-factors, resulting in higher gain \times bandwidth product.

In conclusion, we have investigated the impact of voltage-bias noise on ICTA performance, a noise source that corresponds to pump phase noise in JPAs and is usually negligible there. We have shown experimentally that bias-voltage noise does not degrade ICTA noise as long as the bandwidth of the device is kept larger than the voltage-bias noise distribution so that voltage noise does not cause gain fluctuations. This result implies that improving the bandwidth of the ICTA, e.g. via impedance engineering⁴ of the signal and idler resonators, promises to improve not only the bandwidth but also the noise and robustness of the ICTA. Because it is DC-powered and does not require a pump tone, the ICTA then avoids the risk of saturating the amplifier chain and the need of additional isolation, simplifying the use of quantum-limited amplifiers.

AUTHOR DECLARATIONS

Conflict of Interest

The authors have no conflicts to disclose.

Author Contributions

Ulrich Martel: Conceptualisation (supporting), Formal analysis (equal), Investigation (lead), Methodology (equal), Software (supporting), Visualisation (lead), Writing - original draft (equal), Writing - review & editing (equal). **Romain Albert:** Investigation (supporting), Methodology (supporting), Software (supporting), Writing - review & editing (equal). **Florian Blanchet:** Conceptualisation (supporting), Investigation (supporting), Methodology (supporting), Software (lead). **Joel Griesmar:** Formal analysis (supporting), Investigation (supporting), Methodology (supporting), Software (supporting), Supervision (supporting). **Gabriel Ouellet:** Investigation (supporting), Methodology (supporting), Software (supporting). **Hugo Therrien:** Investigation (supporting), Methodology (supporting). **Naveen Nehra:** Conceptualisation (supporting), Writing - review & editing (supporting). **Nicolas Bourlet:** Formal analysis (supporting), Investigation (supporting), Methodology (supporting), Supervision (supporting), Writing - review & editing (supporting). **Max Hofheinz:** Conceptualisation (lead), Formal analysis (equal), Investigation (supporting), Methodology (equal), Software (supporting), Writing - original draft (equal), Writing - review & editing (equal), Supervision (lead), Funding acquisition (lead), Validation (lead).

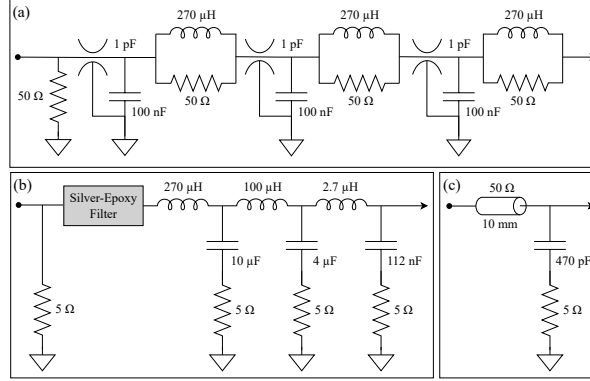


FIG. 5. Voltage bias circuits schematics. (a) 50 Ω biasing circuit. The 1 pF capacitors are feed-through capacitors. (b) 5 Ω biasing circuit. (c) Further filtering for Sample A, on the sample holder.

ACKNOWLEDGMENTS

This work was supported by the Natural Sciences and Engineering Research Council of Canada, the Canada First Research Excellence Fund, the European Union (ERC Starting Grant No. 278203 WiQOJo), and the French Agence Nationale de la Recherche (grant JosePhSCharLi ANR-16-CE92-0033).

DATA AVAILABILITY STATEMENT

The data that support the findings of this study are available from the corresponding author upon reasonable request.

Appendix A: Voltage biasing circuits

Fig. 5 shows the 50 Ω and 5 Ω biasing circuits used in this article. Both connect to the sample holder using SMA connectors. The biasing resistor in both cases absorbs significant power and heats above the base temperature of the fridge. The subsequent filtering stages filter technical noise and noise of the bias resistor and are designed to present a flat output impedance to avoid instabilities of the ICTA.

The high noise configuration uses the 50 Ω biasing resistor²⁵, illustrated in Fig. 5a. Filtering is ensured by three RLC stages in series, with each stage being inside a copper cavity connected via feed-through capacitors to avoid high-frequency leakage.

The medium and low noise configurations use the $5\ \Omega$ biasing circuit²⁶, illustrated in Fig. 5b. This lower resistance yields less thermal voltage noise than the $50\ \Omega$ circuit and the subsequent RLC filter stages have lower cutoff frequency and better high-frequency rejection due a silver epoxy filter stage²⁷.

The low noise configuration uses the $5\ \Omega$ biasing circuit in conjunction with Sample A, which has further filtering as illustrated in Fig. 5c and a final on-chip $100\ \text{pF}$ capacitor. As these filter stages are closer to the actual junctions, they allow a better control of the impedance seen by the junction and prevent parasitic resonances.

Appendix B: Calibration

We calibrate the gain and noise of our readout chain using a Y-factor method, by successively connecting it to a cold and a hot $50\ \Omega$ termination via a cold microwave switch (see Fig. 1). To ensure correct thermalisation of these resistances, they are thermally isolated from the switches via superconducting NbTi coax lines and thermally anchored to, respectively, the mixing chamber stage and the still stage of our dilution refrigerator. Their thermal noise is then acquired in the 4 to 12 GHz band. From these two measurements we calculate the gain of the measurement chain from the switches to the digitizer as well as the noise of the amplification chain referred to the microwave switch. This calibration is used for measuring the ICTA noise.

In order to calibrate ICTA gain measurements we connect the microwave switch to a short circuit and we send in a microwave tone and measure the frequency-dependent reflection coefficient, using the same readout chain as for the noise measurement. The fact that the same readout hardware is used for both measurements allows us to also to accurately calibrate the power delivered to the device because the gain of the chain from switch to digitizer is known.

To extend the calibration from the microwave switch to the device, i.e. calibrate the attenuation of the microwave line between the switch and the device we connect the microwave switch to the ICTA and tune it into an off state, at a bias voltage far from any working point and maximally frustrated SQUID. By doing so, we can consider the device as a nondissipative linear component, fully reflecting the input signal as long as the signal frequency is detuned from the signal mode. Sending a signal and measuring it implies that it travels back and forth between the switch and the device. However, the noise emitted by the device only travels one way through this path. We therefore compute the loss of the transmission line between switch and sample as the square root

of the ratio between the gain calibration using the sample as reflector and the gain calibration using the short circuit as reflector. We observe that the attenuation between the switch and the sample is flat (away from the amplifier mode) and we therefore use a constant attenuation value of 0.498 dB for the full frequency. It is in good agreement with the expected attenuation of the cable at low temperatures.

The final step is to compute the actual ICTA gain and noise and compare it to the quantum limit. To calibrate the gain, we take the ratio of the signals of the ICTA at the working point and in the off state. We measure the noise of the ICTA by performing noise measurement at the working point without any input signal and subtracting noise of the readout chain by subtracting noise at 0 bias voltage where the device does not emit noise. We then divide the measured noise by the calibrated gain from the sample to the digitizer. We can now compare the noise of the device to the quantum limit $|S_{aa}|^2 - 1$.

REFERENCES

- ¹J. Aumentado, *IEEE Microwave Magazine* **21**, 45 (2020).
- ²N. Bergeal, F. Schackert, M. Metcalfe, R. Vijay, V. E. Manucharyan, L. Frunzio, D. E. Prober, R. J. Schoelkopf, S. M. Girvin, and M. H. Devoret, *Nature* **465**, 64 (2010).
- ³J. Y. Mutus, T. C. White, E. Jeffrey, D. Sank, R. Barends, J. Bochmann, Y. Chen, Z. Chen, B. Chiaro, A. Dunsworth, J. Kelly, A. Megrant, C. Neill, P. J. J. O’Malley, P. Roushan, A. Vainsencher, J. Wenner, I. Siddiqi, R. Vijay, A. N. Cleland, and J. M. Martinis, *Applied Physics Letters* **103**, 122602 (2013).
- ⁴T. Roy, S. Kundu, M. Chand, A. M. Vadiraj, A. Ranadive, N. Nehra, M. P. Patankar, J. Aumentado, A. A. Clerk, and R. Vijay, *Applied Physics Letters* **107**, 262601 (2015).
- ⁵N. E. Frattini, V. V. Sivak, A. Lingenfelter, S. Shankar, and M. H. Devoret, *Phys. Rev. Applied* **10**, 054020 (2018).
- ⁶B. Ho Eom, P. K. Day, H. G. LeDuc, and J. Zmuidzinas, *Nature Physics* **8**, 623 (2012).
- ⁷O. Yaakobi, L. Friedland, C. Macklin, and I. Siddiqi, *Phys. Rev. B* **87**, 144301 (2013).
- ⁸C. Bockstiegel, J. Gao, M. R. Vissers, M. Sandberg, S. Chaudhuri, A. Sanders, L. R. Vale, K. D. Irwin, and D. P. Pappas, *Journal of Low Temperature Physics* **176**, 476 (2014).
- ⁹C. Macklin, K. O’Brien, D. Hover, M. E. Schwartz, V. Bolkhovsky, X. Zhang, W. D. Oliver, and I. Siddiqi, *Science* **350**, 307 (2015).

- ¹⁰S. Goldstein, N. Kirsh, E. Svetitsky, Y. Zamir, O. Hachmo, C. E. M. de Oliveira, and N. Katz, *Applied Physics Letters* **116**, 152602 (2020).
- ¹¹M. Esposito, A. Ranadive, L. Planat, and N. Roch, *Applied Physics Letters* **119**, 120501 (2021).
- ¹²D. Hover, Y.-F. Chen, G. J. Ribeill, S. Zhu, S. Sendelbach, and R. McDermott, *Applied Physics Letters* **100**, 063503 (2012).
- ¹³P. Lähteenmäki, V. Vesterinen, J. Hassel, H. Seppä, and P. Hakonen, *Scientific Reports* **2**, 276 (2012).
- ¹⁴S. Jebari, F. Blanchet, A. Grimm, D. Hazra, R. Albert, P. Joyez, D. Vion, D. Estève, F. Portier, and M. Hofheinz, *Nature Electronics* **1**, 223 (2018).
- ¹⁵S. Jebari, *Un amplificateur basé sur le tunneling inélastique de paires de Cooper*, Phd thesis, Université Grenoble Alpes (2017).
- ¹⁶U. Martel, *Développement d'un amplificateur micro-ondes limité quantiquement basé sur l'effet tunnel inélastique de paires de Cooper*, Master's thesis, Université de Sherbrooke (2022).
- ¹⁷B. Abdo, A. Kamal, and M. Devoret, *Phys. Rev. B* **87**, 014508 (2013).
- ¹⁸N. Bergeal, R. Vijay, V. E. Manucharyan, I. Siddiqi, R. J. Schoelkopf, S. M. Girvin, and M. H. Devoret, *Nature Physics* **6**, 296 (2010).
- ¹⁹A. Roy and M. Devoret, *Comptes Rendus Physique* **17**, 740 (2016), quantum microwaves / Micro-ondes quantiques.
- ²⁰A. Paquette, J. Griesmar, G. Lavoie, R. Albert, F. Blanchet, A. Grimm, U. Martel, and M. Hofheinz, *Applied Physics Letters* **121**, 124001 (2022).
- ²¹A. Grimm, S. Jebari, D. Hazra, F. Blanchet, F. Gustavo, J.-L. Thomassin, and M. Hofheinz, *Superconductor Science and Technology* **30**, 105002 (2017).
- ²²G.-L. Ingold and Y. V. Nazarov, "Charge tunneling rates in ultrasmall junctions," in *Single Charge Tunneling: Coulomb Blockade Phenomena In Nanostructures*, edited by H. Grabert and M. H. Devoret (Springer US, Boston, MA, 1992) pp. 21–107.
- ²³M. Hofheinz, F. Portier, Q. Baudouin, P. Joyez, D. Vion, P. Bertet, P. Roche, and D. Esteve, *Phys. Rev. Lett.* **106**, 217005 (2011).
- ²⁴G.-L. Ingold and H. Grabert, *Europhysics Letters (EPL)* **14**, 371 (1991).
- ²⁵F. Blanchet, *Josephson photonics : microwave generation and amplification in the quantum regime*, Phd thesis, Université Grenoble Alpes (2018).
- ²⁶R. Albert, *Multiplication of microwave photons via inelastic Cooper pair tunneling*, Phd thesis, Université Grenoble Alpes (2019).

²⁷C. P. Scheller, S. Heizmann, K. Bedner, D. Giss, M. Meschke, D. M. Zumbühl, J. D. Zimmerman, and A. C. Gossard, *Applied Physics Letters* **104**, 211106 (2014).